Energy Advances

PAPER

View Article Online
View Journal | View Issue

Cite this: *Energy Adv.*, 2026, 5, 754

Fully printed energy storage devices on consumer paper substrates: an eco-friendly approach for a low-cost and disposable smart electronics system

Elena Palmieri,†[ab] Abhinandan Patra,†[c] Giuseppina Polino,[c] Hamed Javanbakht Lomeri,[c] Elisa Casagrande,[c] Giovanni Landi,[d] Luca La Notte,[e] Jenny Baker,[fh] Bas De Jong,[g] Francesca De Rossi,[c] Silvia Orlanducci[b] and Francesca Brunetti*[c]

Received 2nd December 2025,
Accepted 9th February 2026

DOI: 10.1039/d5ya00352k

rsc.li/energy-advances

The integration of electronic devices into wearable applications has revolutionized the way we interact with technology. The utilization of sustainable materials that align with the principles of environmental consciousness makes it more remarkable. In this context, we propose the fabrication of an energy storage device, a supercapacitor, prepared following a "green approach", starting from the substrate used for its fabrication, *i.e.*, various paper-based materials, and continuing through to the final step. The device fabrication was achieved through screen printing, a scalable and efficient technique that enables precise deposition of materials while eliminating waste. The electrode component is carbon-based, offering cost-effectiveness and mechanical durability, while the use of sodium alginate as both the electrolyte and the interlayer represents a significant innovation. By playing a dual role, sodium alginate reduces the need for additional materials, simplifying the manufacturing process and lowering the device's overall environmental impact. Sodium alginate, derived from renewable and sustainable sources, possesses exceptional biocompatibility and eco-friendliness. Its high ion conductivity and excellent film-forming capabilities make it particularly well-suited for flexible and wearable electronic devices. The power of the obtained interdigitated supercapacitor ranged between ~880 μW kg^{-1} and 505 mW kg^{-1}. This approach not only optimizes the device structure but also reduces its ecological footprint, aligning with the growing demand for low-cost green energy technologies and sustainable materials in electronic applications.

1. Introduction

Flexible solid-state supercapacitors (SCs) have attracted great interest due to the growing demand for energy storage devices in modern portable/wearable electronic devices, including mobile phones, laptops, cameras, smartwatches, activity trackers, and health monitoring devices. The increased energy consumption of these smart electronics requires improved energy storage devices with peculiar characteristics: recyclability, biocompatibility, flexibility and low environmental impact both in terms of production and disposal.[1] Batteries based on Li-ion technology might reach 3000 cycles of charging/discharging, but this is not satisfactory for long-term applications.[2] In this context, an alternative is represented by supercapacitors which supply moderate energy density, high power rates and long cycle life.[3] Electric double-layer capacitors (EDLCs) are known to exploit the charge accumulation in the electric double-layer. The mechanism is based on the weak electrostatic interaction of ions from the electrolyte bulk with the electrode

[a] *Consiglio Nazionale delle Ricerche, Istituto per la microelettronica e i microsistemi, via del fosso del cavaliere 1, 00133, Rome, Italy*
[b] *Department of Chemical Science and Technologies, University of Rome Tor Vergata, Via della Ricerca Scientifica 1, 00133, Rome, Italy*
[c] *CHOSE, Department of Electronic Engineering, University of Rome Tor Vergata, via del Politecnico 1, 00133, Rome, Italy. E-mail: francesca.brunett@uniroma2.it*
[d] *ENEA – Research Center Portici – P. le Enrico Fermi, 1 Località Granatello, 80055, Portici (Napoli), Italy*
[e] *ENEA – Research Center Casaccia, via anguillarese 301, 00123, Santa Maria di Galeria (Roma), Italy*
[f] *Faculty of Science and Engineering, Swansea University, Bay Campus, SA1 8EN, UK*
[g] *Department of Biotechnology, Chemistry and Pharmacy, University of Siena, Via A. Moro 2, Siena, 53100, Italy*
[h] *Faculty of Engineering and Design, University of Bath, Claverton Down, Bath, BA2 7AY, UK*
† These authors contributed equally.

surface.[4] Unlike batteries, this kind of energy storage device can store the charge physically, and the lack of electrochemical reactions ensures very high power (with a response time of up to 1 s) and a cyclability of 100 000 cycles.[3] When designing an SC, there are many crucial aspects to be taken into consideration, starting from the substrate to be used for the fabrication of the device, to the choice of the electrode and electrolyte and finally, the suitable technique for the fabrication. As for the substrate, commonly used materials include polymers such as polyethylene terephthalate (PET), polyimide (PI), and polyethylene naphthalate (PEN)[5,6] which offer excellent mechanical flexibility and thermal stability, enabling the fabrication of flexible and wearable energy storage devices. They provide a robust template for electrode materials, maintaining structural integrity during bending or stretching. Notwithstanding their proven efficacy and pervasive deployment, the necessity for environmentally benign alternatives persists. Significant research efforts[7,8] are now being directed towards the development of energy storage devices utilising paper and paper-like materials. These materials offer a number of significant advantages, including flexibility, lightweight and broad availability, which collectively contribute to a cost-effective and environmentally friendly fabrication process. Despite the fact that paper substrates typically display reduced mechanical strength and thermal stability compared to conventional materials, and that their overall processability is more constrained, notable outcomes have been attained.[9]

To overcome the lower energy density of SCs, in the last few decades, research on electrodes for SCs began with the investigation of carbon- and conducting polymer (CP)-based materials.[1,10] Carbon-based materials used in the fabrication of supercapacitor electrodes exhibit versatile properties, *i.e.* a high specific surface area and a well-defined porosity, making them the most popular choice for electrochemical capacitor applications. Moreover, they are suitable for low-cost room temperature techniques such as screen printing.[11,12] It is well-known that the textural and structural properties of the electrode material play a central role in the final performance of an electrochemical capacitor. Furthermore, it is possible to use activated carbon normally obtained from biomass.[13,14] Likewise, hydrogels possess promising features, such as stretchability, foldability, and even self-healing ability, for application in sustainable portable/wearable electronics[15–17] and can be employed in the fabrication of both electrodes and electrolytes for devices such as supercapacitors.[18–28] In recent years, it has been demonstrated that there is a possibility to realize electrolytes using an environment-friendly and biocompatible polysaccharide, taking advantage of the natural porous structure present in the seaweed, mainly Na- (sodium alginate) and K-derivatives (usually carrageenan—a potassium-rich carbohydrate), homogeneously distributed in the bulk of this biomass. The use of porous hydrogel nanostructures provides high flexibility and combines several properties such as easy processability, reduction of the device cost, improved solid–liquid interface, larger electrochemically active surface area, short pathways for charge/mass transport and reliable behaviour during bending cycles.[22,24] For supercapacitors, electrolytes can be categorized into aqueous, organic, and ionic types, each with distinct advantages and limitations.[29–31] Aqueous electrolytes offer high conductivity but have a low dissociation voltage. Organic electrolytes provide higher voltage and a broader temperature range but lower conductivity and higher costs. Ionic electrolytes, while stable at higher voltages, exhibit lower conductivity than aqueous or organic electrolytes.[31] Sodium alginate emerges as a sustainable alternative, forming thick, stable gels when combined with metal ions, enabling safe and efficient sodium-ion-based energy storage. Its natural origin, low cost, and excellent film-forming properties make it ideal for environmentally friendly energy applications.[23,24,32,33]

In this study, carbon-based interdigitated supercapacitors were fabricated on paper-derived substrates, including copy paper and different types of consumer paper. These substrates were chosen for their biocompatibility, low cost, and suitability for smart electronics applications. Sodium alginate was employed as a functional interlayer on top of the carbon electrode and as the electrolyte. Comparative analysis of the different paper types revealed that the surface morphology, the texture and the overall structure of the substrate influence the total capacitance of the supercapacitor. We achieved a maximum specific areal capacitance of $\sim$70 μF cm^{-2} and a gravimetric capacitance of $\sim$280 μF g^{-1} with copy paper. These findings present exciting prospects for the utilization of diverse paper substrates in the development of high-performance supercapacitors for energy storage and smart electronics applications.

2. Experimental section

2.1 Materials

Carbon-based electrodes were realized using highly conductive thermoplastic carbon paste (Dycotec DM-CAP-4701S). This paste allows fast drying at low temperature ($<$100 °C) with a sheet resistance of $<$10 Ω//25 μm. The electrolyte was prepared using 0.15 g of Na alginate (Sigma Aldrich) dissolved in 6 ml of deionized water; the functionalization layer that acts as an interlayer was prepared using 1.5 g of Na alginate dissolved in 50 ml of deionized water. Both solutions were stirred for 6 hours at room temperature before use. The Na-alginate solution used as the electrolyte showed a slightly lower conductivity, 4.5 mS cm^{-1} at 20 °C, compared to the interlayer solution (8.7 mS cm^{-1} at 20 °C), due to the lower polymer amount. Acid-free copy paper with alkaline reserve was provided by Cartiere Miliani Fabriano, and disposable paper substrates were supplied by Essity AB industries.

2.2 Device fabrication

The initial stage of the fabrication process for supercapacitors entails the screen printing of the carbon electrodes (Baccini Screen Printers) utilising a printing screen of dimensions 380 × 460 mm with a mesh of 45 μm. The total active area of the electrode was found to be 2.88 cm^2, with the measured fingers having a width of $\sim$1 mm and a length of $\sim$15 mm. In Fig. 1a,

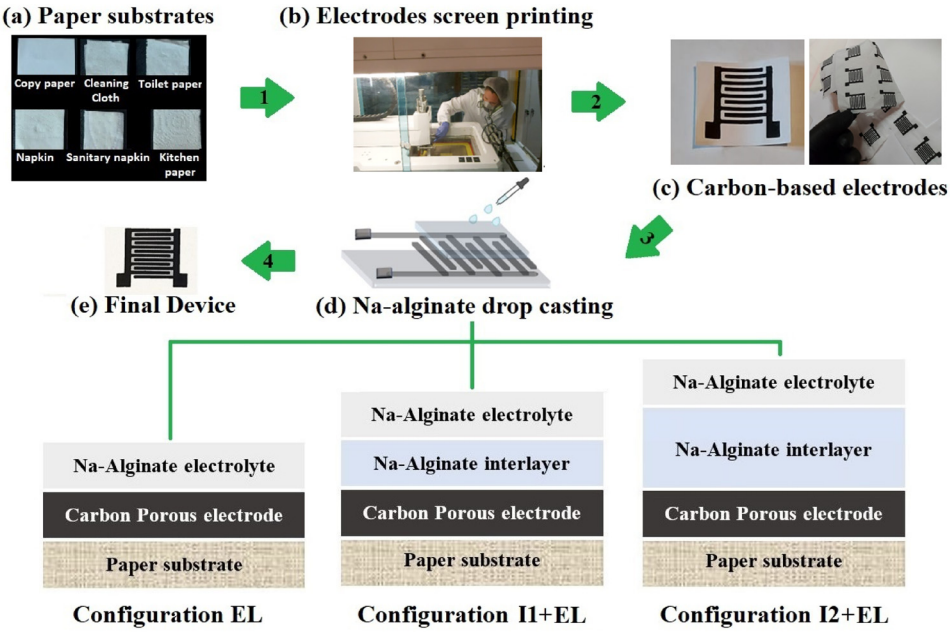

Fig. 1 The fabrication process of printed supercapacitors: (a) paper substrates employed in the experiments: copy paper, cleaning cloth, toilet paper, napkin, sanitary napkin, and kitchen paper; (b) screen printing of carbon electrodes; (c) printed carbon-based electrodes on copy and disposable paper; (d) deposition of the sodium alginate interlayer and/or the electrode *via* drop casting; and (e) final device. Inset in (d): configuration of the three different supercapacitors investigated; configuration EL: electrolyte applied directly on the electrode surface; configuration I1 + EL: electrolyte applied on top of the Na-alginate interlayer (200 μl); and configuration I2 + EL: electrolyte applied on top of the Na-alginate interlayer (400 μl).

the paper substrates used in the experiments are shown, and the fabrication of the interdigitated planar structure based on a carbon-based electrode on the top of different large-area paper substrates is shown in Fig. 1b and c. After the deposition, the electrodes were sintered in an oven at 80 °C for 1 h and cut to obtain substrates with an area of 4 cm^2. The deposition of the electrolyte and interlayer sodium alginate was performed by the drop casting method (Fig. 1d) and then dried at room temperature overnight in a controlled ambient humidity of 50% RH. More specifically, three different configurations of the supercapacitor were investigated, as reported in the inset of Fig. 1d. In the first case, Na-alginate was used at a lower concentration (2.4%$_w$, 600 μl) as an electrolyte directly in contact with the electrode (Fig. 1d-EL). In the other two cases, an interlayer of Na-alginate (2.9%$_w$) was deposited before the deposition of the electrolyte. Two interlayers of different thicknesses were investigated (200 μl, Fig. 1d-I1 + EL, and 400 μl, Fig. 1d-I2 + EL).

The deposition of the electrolyte, both for the I1 + EL and the I2 + EL configurations, was performed after the complete drying of the interlayer. For all three configurations, the devices were characterised soon after the deposition of the electrolyte (wet) and the day after (dry).

2.3 Rheological characterization of the electrolyte and interlayer

Rheological characterization of the Na-alginate-based electrolyte and interlayer was performed using an AR 2000 rheometer (TA Instruments) with a cone and plate measurement geometry, where the cone rotates, imposing a homogeneous strain through the sample, which is placed on the fixed plate. Specifically, a 60 mm diameter 2° acrylic cone was used. The viscosity–shear rate profiles, referred to as 'flow curves', were determined at 25 °C, with the shear rate ranging from 0.1 to 1000 s^{-1}.

2.4 Morphological characterization

Scanning electron microscopy (SEM, TESCAN MIRA) was performed to analyse the morphologies of the various paper substrates and the carbon electrodes interfaced with Na alginate. The thickness was measured using a feeler gauge (Digital Thickness Gauge FD 50, Käfer).

2.5 Materials and composition analysis

A sample of carbon ink was subjected to simultaneous thermal analysis (STA). Nitrogen adsorption was carried out using a Micromeritics TriStar Surface analyser with isotherms measured at −196 °C; the pre-treatment temperature and time were 80 °C for the ink and 400 °C for the powder for 8 hours. 400 °C was chosen as the pre-treatment temperature for the powder material since STA analysis determined that the binder was removed from the ink at temperatures above 375 °C. The BET (Brunauer–Emmett–Teller) surface area calculations were performed on results between partial pressures of 0.08 and 0.25.[34]

2.6 Electrochemical characterization

The electrochemical performances of the devices were measured using cyclic voltammetry (CV), charge–discharge (CH–DIS) measurement and electrochemical impedance spectroscopy

(EIS) on a commercial platform (Arkeo – Cicci Research srl) composed of a potentiostat–galvanostat module (up to 1 MHz of bandwidth), a thermal-vacuum stage and a multichannel not-multiplexed module. Specific capacitance (C_s), specific energy (E), and specific power (P) are calculated using the following equations:[35,36]

$$C_{s\text{-CV}} = \frac{\int I \mathrm{d}V}{v \times m \times \Delta V} \quad (1)$$

$$C_{s\text{-CH-DIS}} = \frac{I \times \Delta T}{m \times \Delta V} \quad (2)$$

$$E = \frac{1}{2} \times CV^2 \times \frac{1}{3600} \quad (3)$$

$$P = \frac{E}{\Delta T} \times 3600 \quad (4)$$

where I is the current, v is the scan rate, m is the mass loading, V is the potential window, and T is the discharge time.

The aforementioned formulas are expressed in terms of mass loading.

The capacitance by area was calculated using eqn (5) and (6).

$$C_{s\text{-CV}} = \frac{\int I \mathrm{d}V}{v \times A \times \Delta V} \quad (5)$$

$$C_{s\text{-CH-DIS}} = \frac{I \times \Delta T}{A \times \Delta V} \quad (6)$$

where A is the active area of the electrode.

3. Results and discussion

We studied the rheological behavior of Na-alginate solutions to assess their suitability for common coating and printing techniques. Viscosity is a crucial parameter for understanding fluid deformation under shear and its resistance to mechanical stress. Shear rates vary depending on the technique, ranging from 0.1 to 10 for drop casting to 10–1 000 000 s^{-1} for high-speed blade coating.[37] Fig. S1 of the SI shows the flow curves for alginate bio-hydrogels, which display typical non-Newtonian shear-thinning behavior, common in polymer solutions due to polymer alignment during shear. We used the Cross model to fit the curves and determine the zero-rate viscosity, finding values of 0.21 Pa s for the interlayer solution and 0.18 Pa s for the electrolyte. As expected, the interlayer solution, with a higher polymer concentration, exhibited slightly higher viscosity than the electrolyte solution. Both solutions remained stable within the tested shear rate range, making them suitable for various coating techniques like blade coating, dip-coating, and drop casting, which were used for the fabrication of the device.

To evaluate the performance of carbon-based and alginate-based materials as a function of the substrate's porosity and hygroscopicity, different kinds of disposable cellulose-based wipers and cloths (reported in Fig. 1a) were taken into consideration. Prior to the fabrication of the supercapacitor, morphological characterization of the various types of paper was performed to determine which were more suitable for the fabrication of a printed device. These types of paper, despite the fact that all are cellulose-based materials, differ from one another in terms of robustness, porosity, and fibre composition. More specifically, the selection of the paper for the fabrication of the devices was based on its compatibility with uniform screen-printing deposition of the carbon electrodes. Paper presenting both artificial and native fibres was excluded, as the presence of different kinds of fibres could affect the final quality of the deposition due to differences in affinity (wettability, adsorption, adhesion, *etc.*) between fibres and carbon pastes.[38,39] The inhomogeneous cohesion between the fibre and the ink is likely to end up in exfoliation, cracking, or other undesirable phenomena which could eventually lead to affecting the performance of the final device. Regarding substrate robustness, an excessive thinness and the presence of holes and voids would lead to a highly uneven deposition of the electrode material, compromising the efficient printing of the electrode pattern and, thus, the functionality of the device. From the investigation performed, among the many types of paper characterised, the choice fell on Cleaning Cloth®, Tork® napkins, and Floralys® kitchen paper supplied by Essity, and their SEM characterization results are shown in Fig. 2: each paper was observed at different magnifications, from the lower (left column) to the higher magnification (right column). Common copy paper was used as the reference substrate due to its robustness and high compatibility with printing techniques[28] and its SEM characterization results are also shown in Fig. 2a.

Fig. 2a illustrates the typical fibrous structure of copy paper, observed under three different magnifications. The fibres have an average width of 15 μm. In the case of napkin Tork® (Fig. 2b), it is possible to notice a rather compact structure. From the SEM image at lower magnification, a knitted arrangement in the distribution of the fibres can be observed. Fibres show an average width of around 15 μm. With regard to Floralys® kitchen paper (Fig. 2c), a relatively compact structure can be observed. From the SEM image at lower magnification, a curled/wave-like arrangement can be observed. Fibres show an average width of around 15 μm. As for the cleaning cloth® (Fig. 2d), from the SEM image at lower magnification, a rather disordered fibrous structure can be observed, characterized by only native cellulose fibres, with an average width of around 15–20 μm. At higher magnification, a dotted pattern can be observed, which could be due to industrial processing. Hence, based on the SEM analysis, cleaning cloth® paper was not used in the following experiments because of its disorganized structure. The morphology of bare carbon-based electrodes, and carbon electrodes coated with electrolyte and with an interlayer and electrolyte, was investigated. Fig. 3a shows the morphology of the electrodes deposited on different paper substrates, revealing a compact structure of all the carbon electrodes regardless of the type of cellulose matrix. As reported in the SI (Fig. S2), in all cases, the carbon electrode shows a granular morphology. The presence of the electrolyte (Fig. 3b) increases the homogeneity of the surface of the device, even though some

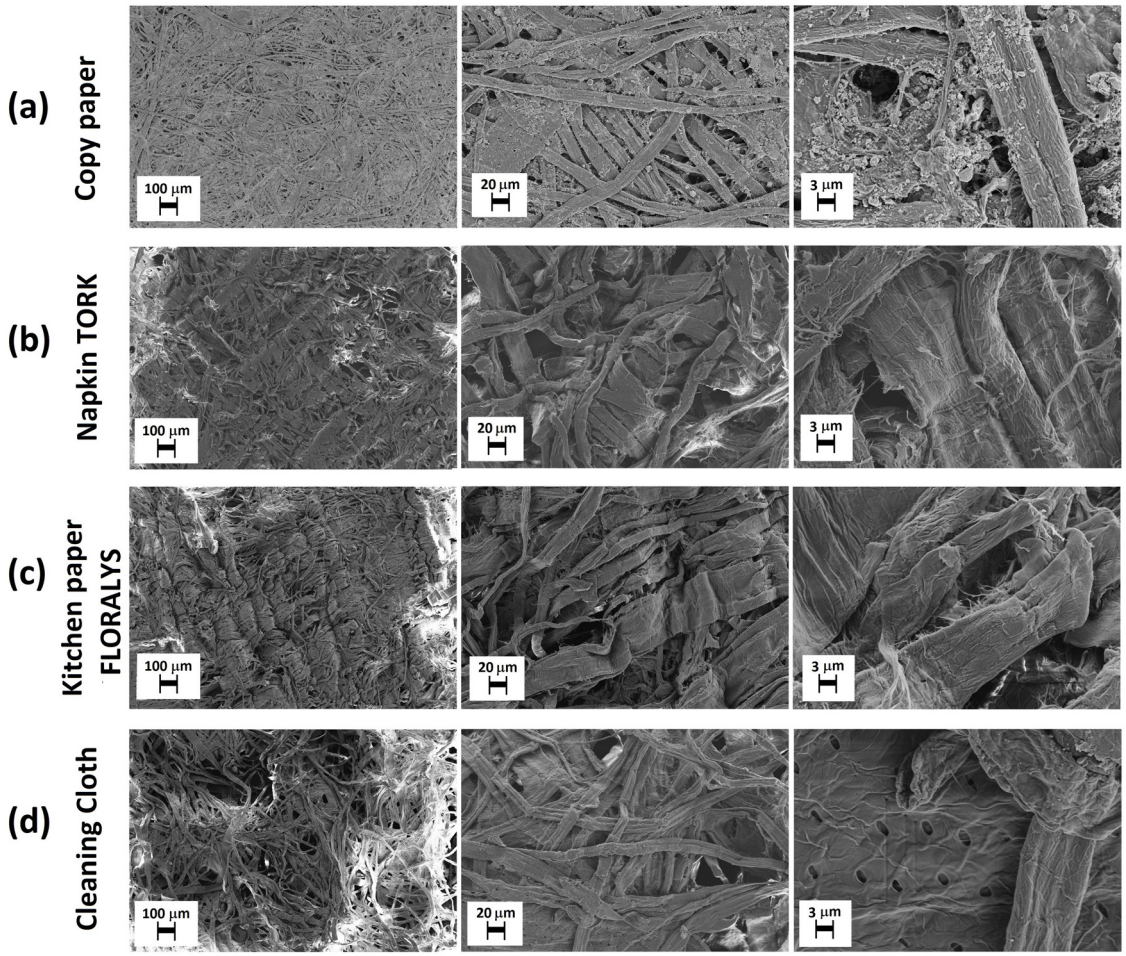

Fig. 2 SEM characterization of (a) copy paper; (b) napkin TORK; (c) kitchen paper FLORALYS; and (d) cleaning cloth.

surface defects such as bubbles and delamination areas can be observed. The use of an interlayer on the top of the carbon electrode (Fig. 3c) leads to an even more uniform morphology. In this case, some bubbles were also observed, likely caused by air trapped during the coating process. The interlayer interface on the carbon electrode enables a significantly improved and more uniform deposition of the electrolyte. No notable morphological differences were observed among the various types of paper, as the interlayer + electrolyte system effectively envelops and covers the paper's fibrous structure.

Additionally, we performed a surface area analysis on both the carbon ink and the carbon active material (*e.g.* the powder remaining after thermal removal of the polymeric binder). Whilst it is not the purpose of this work to optimise the carbon electrode, it is important to measure the surface area to allow comparison with other literature reports. Most research focuses on the surface area of the active material, but this is only part of the understanding.[40] For this material, the isotherms show limited hysteresis (Fig. 4) and indicate slit-like pores typical of graphitic materials. The surface area of the electrode (including binder) was 2.7 $m^2\ g^{-1}$ whereas the surface area of the active carbon material was 23.2 $m^2\ g^{-1}$ denoting a 10-fold reduction in the surface area after the introduction of the binder (Fig. 4). This is a typical behaviour of inks where the binder can significantly reduce the apparent surface area of a coating and is a compromise between ink printability/electrode robustness and the available active surface area.[41,42]

Consequently, the full potential of the active material in terms of the surface area cannot be fully realized. Despite the surface area of the electrode being orders of magnitude lower than that of the active material, the devices exhibit noteworthy performance owing to the high paper surface area, especially when compared with substrates like glass, silicon, PET, PI, PEN, and others.[32,43]

Supercapacitors were fabricated on all four substrates: copy paper, napkin TORK, kitchen paper FLORALYS and cleaning cloth; however, the thin and delicate nature of napkin TORK made it prone to damage during the screen-printing process, presenting significant challenges in device fabrication. The three configurations (EL, I1 + EL, and I2 + EL) were first examined on copy paper, which was used as the reference substrate. The performance of the devices was tested for all three configurations both before and after the electrolyte drying process, referred to as wet and dry devices, respectively. In the case of dry-device measurements, the electrolyte was allowed to dry overnight at room temperature before testing. In Table S1,

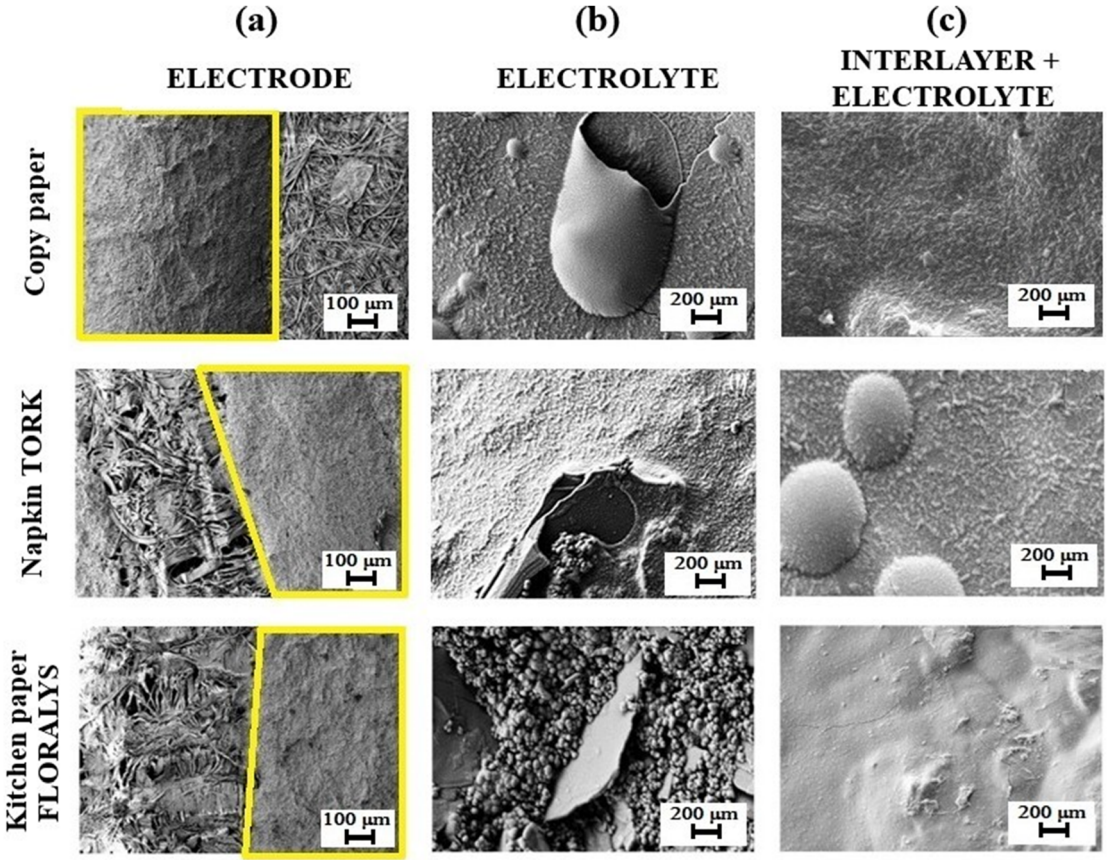

Fig. 3 SEM micrograph of (a) carbon electrode (yellow box), (b) carbon electrode + Na alginate electrolyte, (c) carbon electrode + Na alginate interlayer + Na alginate electrolyte deposited on Copy paper, napkin paper TORK, and kitchen paper FLORALYS.

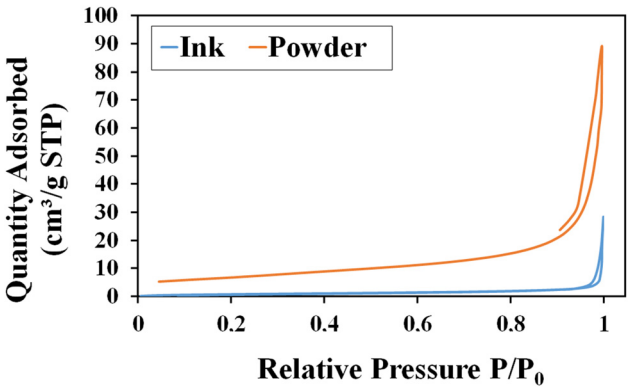

Fig. 4 Isotherms of the carbon ink and the ink active materials (powder) once the binder contained in the ink has been removed.

the thicknesses of the device at the various configurations are reported.

The CV profiles of devices on copy paper were recorded in the range of 10 to 100 mV s^{-1} (Fig. 5a–c), for all the configurations, both wet and dry. Fig. 5d displays the comparative CV graphs at 80 mV s^{-1} for all the configurations. The CV indicated the capacitive behavior of the devices, showcasing excellent rate capability and reversibility across all the investigated scan rates. A growing capacitive behavior is evident with the presence of the interlayer, observed in both the wet and dry devices. As expected, superior performances were obtained in the wet devices, due to major ionic mobility and availability at the electrode surface. Nevertheless, acceptable capacitive behavior was still achieved with the dry devices, particularly in the case of configuration with the interlayer (Fig. 5b and c). It should be noted that subtle alterations in the CV curves are noticeable at extremely low scan rates with small oxidation and reduction peaks, which could be ascribed to the surface faradaic reactions taking place in the electrode and the electrolyte interface. This phenomenon can be due to the intercalation/deintercalation of electrolytic ions Na^+ (ref. 44 and 45) during the charge/discharge cycles. At higher scan rates, the capacitive contribution becomes predominant,[46] and these alterations are no longer present. The capacitance values for all three configurations for both wet and dry devices are reported in Table 1. From the collected data, one can conclude that the presence of the interlayer improves the performance of the device. However, no significant improvement was observed in increasing the thickness of the interlayer. In fact, similar values were found for the configurations I1 + EL and I2 + EL. Additionally, the presence of the interlayer has a more pronounced impact on the performance of the dry devices compared to the wet devices. The power law has been employed to analyse the faradaic redox reaction, which influences the diffusion-

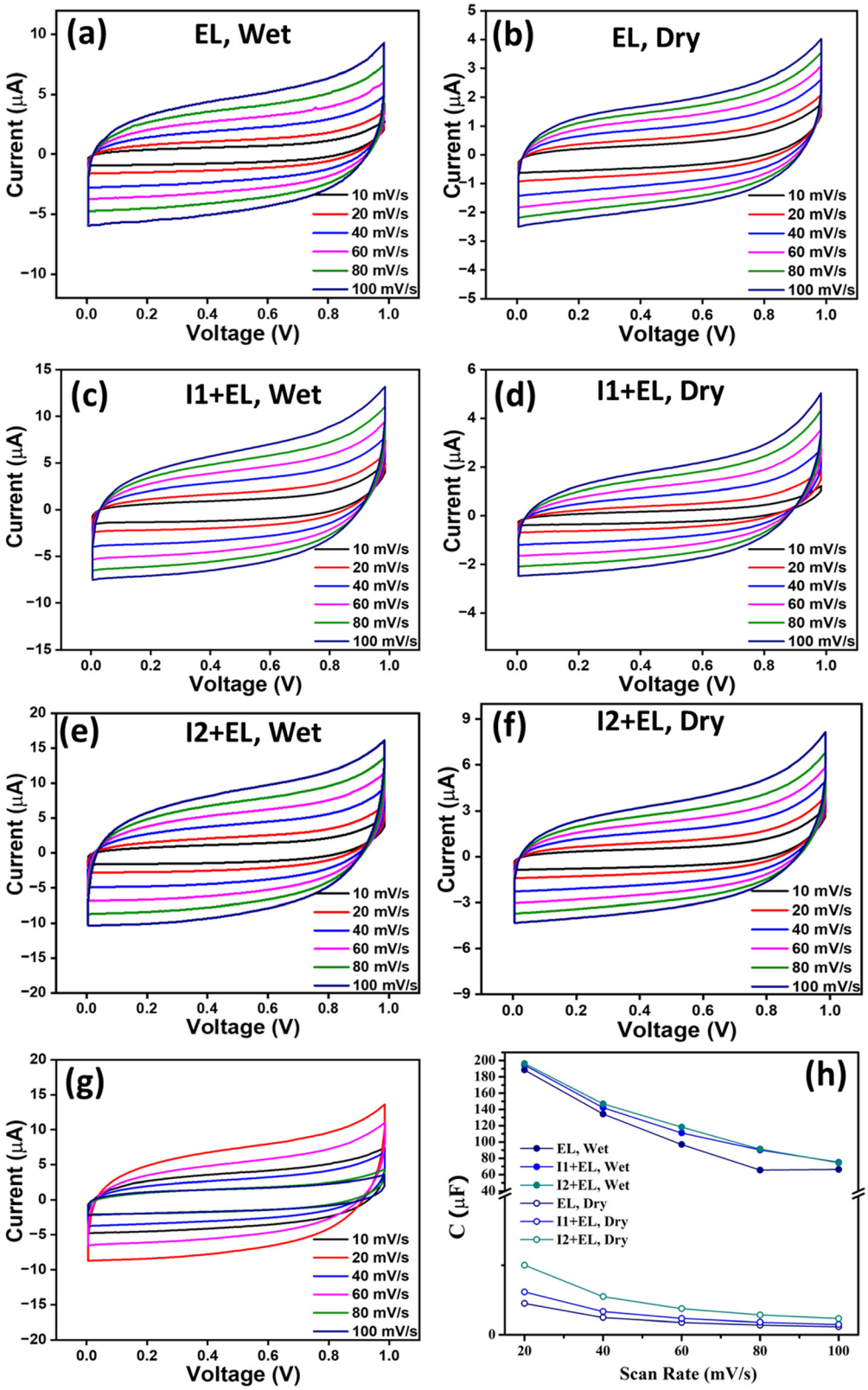

Fig. 5 CV characterization for copy paper-based devices, with the three configurations tested (a) and (b) at various scan rates for the configuration EL (only electrolyte), wet and dry devices; (c) and (d) at various scan rates for the I1 + EL (interlayer 200 μl + electrolyte), wet and dry devices; (e) and (f) at various scan rates for the I2 + EL (interlayer 400 μl + electrolyte), wet and dry devices; (g) at a fixed scan rate of 80 mV s^{-1}, for the wet and dry devices; and (h) capacitance as a function of the scan rate for the various configurations tested.

Table 1 Performance achieved for various paper substrates, with different device configurations. n.a. = not applicable, in the case of a non-functioning device or configuration

		C (μF)	C_{sp} (μF cm^{-2})	C_{sp} (μF g^{-1})	P_{area} (μW cm^{-2})	P_{mass} (μW g^{-1})	E_{area} (μWh cm^{-2})	E_{mass} (μWh kg^{-1})	Q (μAh)
Copy paper	EL, wet	188.4	65.4	306.4	21.8	102.0	36.3×10^{-3}	170.2	0.105
	I1 + EL, wet	194.4	67.5	236.8	13.5	47.4	36.9×10^{-3}	131.6	0.108
	I2 + EL, wet	196.3	68.2	191.1	13.6	38.2	36.5×10^{-3}	106.2	0.109
	EL, dry	5.3	1.9	354.7	1.1	202.7	1.02×10^{-3}	197.0	0.0030
	I1 + EL, dry	7.78	2.7	370.5	4.2	570.0	1.50×10^{-3}	205.8	0.0043
	I2 + EL, dry	10.0	3.5	370.7	4.1	436.2	1.93×10^{-3}	206.0	0.0056
Kitchen paper	EL, wet	290.5	100.8	472.3	16.1	75.6	56.0×10^{-3}	262.4	0.161
	I1 + EL, wet	319.3	110.9	310.9	44.3	124.4	61.6×10^{-3}	172.7	0.177
	EL, dry	0.71	0.2	47.1	n.a.	n.a.	0.1×10^{-3}	26.1	0.00040
	I1 + EL, dry	8.26	2.9	305.9	4.6	489.5	1.6×10^{-3}	170.0	0.0046
Napkin paper	EL, wet	287.5	99.8	467.5	79.9	374.0	55.5×10^{-3}	259.7	0.160
	I1 + EL, wet	180.9	62.8	176.1	251.3	704.6	34.9×10^{-3}	97.8	0.100
	EL, dry	n.a.	n.a.	n.a.	n.a.	n.a.	n.a.	n.a.	n.a.
	I1 + EL, dry	3.47	1.2	128.5	n.a.	n.a.	0.7×10^{-3}	71.4	0.00193

controlled process, as well as the surface-bound supercapacitive kinetics that determine the capacitive response. These contributions have been quantified using the equations provided below.[47,48]

$$i = a\nu^b \tag{7}$$

$$\log i = b \log \nu + \log a \tag{8}$$

All parameters used here retain their standard meanings: i represents the current, ν denotes the scan rate, and a and b are the variables. The value of b indicates the dominant contribution, $b = 0.5$ signifies a diffusion-controlled process, while $b = 1$ suggests a capacitive contribution. The value of 'b' between 0.5 and 1 implies a mixed contribution from both mechanisms.

$$i(V) = k_1 + k_2\nu^{1/2} \tag{9}$$

$$i(V)/\nu^{1/2} = k_1\nu^{1/2} + k_2 \tag{10}$$

The quantitative assessment of the contribution was carried out using the above equation in conjunction with Dunn's method. In this analysis, k_1 and k_2 correspond to the slope and intercept values derived from the linear fitting. At a scan rate of 40 mV s^{-1}, the capacitive contribution was observed to be 84.5%, while the diffusion-controlled component accounted for 14.5% (Fig. S3a). Likewise, as the scan rate decreased from 40 to 20 mV s^{-1}, the capacitive contribution gradually declined from 84.5% to 80%; similarly, when the scan rate increased the capacitive contribution also increased, confirming the predominantly capacitive nature of the electrode over battery-type behaviour (Fig. S3b).

The charge–discharge plots for copy paper in the wet configuration are reported in Fig. 6a–c, and further characterization is reported in Fig. S4 of the SI. From these results, we extracted the power performance of each architecture: faster charge–discharge in the case of interlayer-based devices in dry devices has been observed, leading to a dramatic increase in Power (Table 1) with respect to wet devices. The stability up to 5000 charge–discharge[49] cycles was investigated for all three configurations, both wet and dry, and graphs are reported in Fig. 6d. It is evident that in wet devices, the capacitance decreases as the electrolyte dries out. Once the electrolyte is fully dried, the capacitance values stabilize, although at significantly lower levels (up to −80% after 5000 cycles). This behavior is more stable for configurations with the interlayer, which exhibit a more gradual decrease in capacitance over time. Similarly, in dry devices, the configurations with the interlayer demonstrate a more stable response, showing around a 40% increase in capacitance. In the configuration without the interlayer, around an 80% loss in capacitance is observed after 5000 cycles with more than 96% of coulombic efficiency.

Fig. S5 presents the results of the EIS investigation for the three configurations. The figure highlights a shift in the equivalent series resistance (ESR), estimated from the x-intercept of the EIS spectra, towards lower resistance values with the incorporation of I1 and I2. This reduction in ESR enhances the supercapacitor's energy storage and delivery capabilities, thereby improving its overall energy performance. In the case of copy paper, the data demonstrate that the presence of the interlayer significantly enhances capacitance behaviour. The improved electrochemical performance observed in the copy paper with the I2 + EL configuration can be attributed to the lower solution resistance (R_s) and charge transfer resistance (R_{ct}) of the electrode compared to other configurations. This improvement is likely due to the increased active surface area facilitated by this specific configuration.[19,50,51] This finding aligns with previous literature on the role of sodium alginate in relation to carbon electrodes.[1,32] After examining the role of the interlayer in the context of the reference copy paper, we proceeded to evaluate the device performance using the other types of paper. Given that no significant difference was observed among the configurations with different thicknesses of the interlayer, the I1 + EL configuration becomes the preferred choice in terms of both device performance and cost-effectiveness. Consequently, the EL and I1 + EL configurations were studied for the other two types of paper substrates.

In Fig. S6, we present the comparison of the CV curves within the potential window of −1 to 1 V for dry devices and

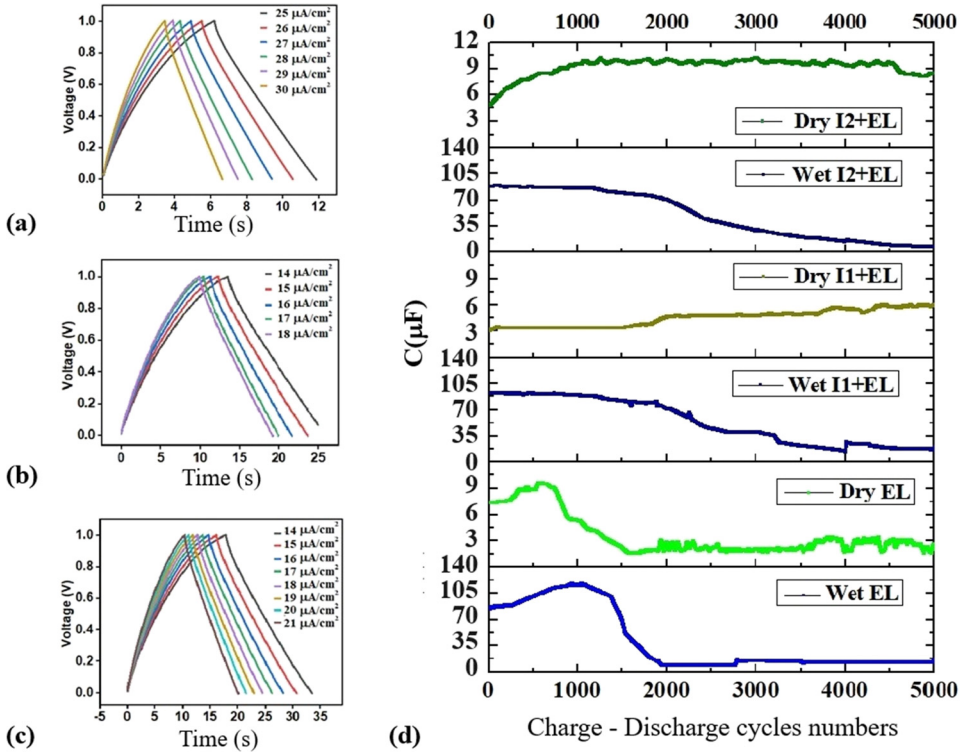

Fig. 6 Charge–discharge for reference devices on copy paper (a) wet EL configuration, (b) wet I1 + EL, and (c) wet I2 + EL, (d) cyclic stability up to 5000 cycles for the EL configuration, wet and dry, I1 + EL configuration, wet and dry, and I2 + EL configuration, wet and dry.

−0.75 to 0.75 V for wet devices at a scan rate of 100 mV s^{-1} for both the kitchen paper and napkin paper, and the data are summarized in Table 1. This experiment was performed to observe the electrochemical response of the devices during both the negative and positive scans, ensuring a complete assessment of their charge–discharge behaviour and verifying the symmetry of the CV profiles across the potential window. As evident from the data, the porosity and absorbent properties of the paper significantly influence the capacitive behaviour. Both devices on the kitchen paper and napkin paper exhibit slightly higher capacities than that on the copy paper.

For the kitchen paper, the interlayer improves device performance, especially in the dry configuration. Conversely, for the napkin paper, the presence of the interlayer reduces device performance in the wet configuration. This effect is attributed to the delicate nature of the paper; the interlayer and electrolyte depositions during device fabrication exert excessive stress on the paper, causing it to swell during deposition and shrink while drying, leading to deformation of the paper substrate, ultimately affecting device functionality. However, once again, the interlayer has a noteworthy positive effect on the dry devices. In fact, while a functioning dry device could not be achieved with the EL configuration, decent performance was obtained with the I1 + EL configuration.

In Fig. S7, we present a comparison of the charge–discharge plots for devices prepared on commercial paper substrates. It was not possible to obtain charge–discharge cycles for supercapacitors in the EL dry configuration for either the kitchen or napkin paper. However, for the dry configuration, we successfully achieved charge–discharge cycles for the I1 + EL configuration using the kitchen paper. For these types of paper, the configuration incorporating the interlayer demonstrated faster cycles compared to the configuration without it, which contrasts with the behaviour observed on the copy paper. This is probably due to the intrinsic morphological differences between these paper samples. Fig. S8 shows the CV and GCD curves of the devices connected in series and parallel

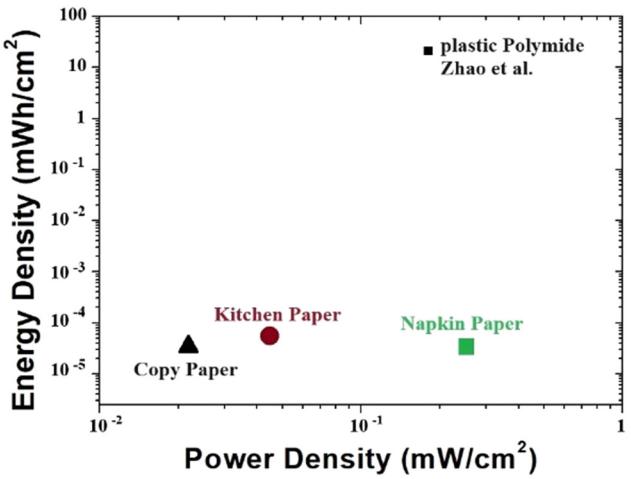

Fig. 7 Ragone plot of the printed supercapacitors on paper and the reference device on plastic from the literature.

configuration signifying the reproducibility of the devices and their application in real time.

The performances of our devices are reported in the Ragone plot (Fig. 7) as well as in Table S2 in the SI, comparing them with the recent study proposed by Zhao *et al.* that used the same electrolyte on plastic polyimide, achieving a power density of 0.18 mW cm^{-2} and an energy density of 21.20 μWh cm^{-2}.[23] Building on this work, we are the first to successfully develop supercapacitors on commercial and disposable paper substrates using an Na-alginate eco-friendly hydrogel demonstrating the critical importance of the combination of substrate porosity and the device architecture that influence the overall performance of the device.

4. Conclusion

In this preliminary investigation, we have successfully demonstrated the feasibility of fabricating energy storage devices on disposable and biodegradable paper substrates commonly used in everyday life. We used an Na-alginate eco-friendly hydrogel as an electrolyte, and we were able to tune the architecture and performance of the devices by using Na-alginate at different concentrations as an interlayer between the carbon-based electrodes and the electrolytic layer. Furthermore, we confirmed the compatibility of cellulose-based substrate materials with the fabrication of electrical devices using large-area printing methods and biocompatible, biodegradable raw materials. This work lays the groundwork for developing smart supercapacitors on unconventional and flexible substrates. We achieved a power density of 251 μW cm^{-2} and an energy density of 62 nWh cm^{-2} on paper substrates, without resorting to harsh chemicals or unsustainable materials, underscoring the potential for the much-needed high-performing, environmentally friendly energy storage solutions.

Conflicts of interest

There are no conflicts to declare.

Data availability

The supporting data have been provided as part of the supplementary information (SI). Supplementary information: Fig. S1–S8 showing SEM images, electrochemical performance and Table S1 showing a comparison of the figure of merit with the state of the art. See DOI: https://doi.org/10.1039/d5ya00352k. The raw data supporting this article can be accessed at https://zenodo.org/records/18471292.

Acknowledgements

The authors acknowledge the support from the European H2020 project, ''Wearable Applications enabled by electronic Systems on Paper (WASP)'' (no. 825213). We acknowledge funding from the UKRI – EPSRC through TReFCo EP/W019167/1 (J.B.).

References

1 M. M. Pérez-Madrigal, F. Estrany, E. Armelin, D. D. Díaz and C. Alemán, Towards sustainable solid-state supercapacitors: electroactive conducting polymers combined with biohydrogels, *J. Mater. Chem. A*, 2016, **4**, 1792–1805.
2 Y. Jiang and W. Song, Predicting the Cycle Life of Lithium-Ion Batteries Using Data-Driven Machine Learning Based on Discharge Voltage Curves, *Batteries*, 2023, **9**, 413.
3 H. Gul, A.-H. A. Shah and S. Bilal, Achieving Ultrahigh Cycling Stability and Extended Potential Window for Supercapacitors through Asymmetric Combination of Conductive Polymer Nanocomposite and Activated Carbon, *Polymers*, 2019, **11**, 1678.
4 A. Patra, *et al.*, Understanding the charge storage mechanism of supercapacitors: in situ/operando spectroscopic approaches and theoretical investigations, *J. Mater. Chem. A*, 2021, **9**, 25852–25891.
5 Latest advances in substrates for flexible electronics – MacDonald – 2007 – Journal of the Society for Information Display – Wiley Online Library. https://sid.onlinelibrary.wiley.com/doi/abs/10.1889/1.2825093.
6 M. Hassan, *et al.*, Significance of Flexible Substrates for Wearable and Implantable Devices: Recent Advances and Perspectives, *Adv. Mater. Technol.*, 2022, **7**, 2100773.
7 M. Beg, *et al.*, Paper Supercapacitor Developed Using a Manganese Dioxide/Carbon Black Composite and a Water Hyacinth Cellulose Nanofiber-Based Bilayer Separator, *ACS Appl. Mater. Interfaces*, 2023, **15**, 51100–51109.
8 K. Dissanayake and D. Kularatna-Abeywardana, A review of supercapacitors: Materials, technology, challenges, and renewable energy applications, *J. Energy Storage*, 2024, **96**, 112563.
9 A. Thakur and P. Devi, Paper-based flexible devices for energy harvesting, conversion and storage applications: A review, *Nano Energy*, 2022, **94**, 106927.
10 E. Raymundo-Piñero, F. Leroux and F. Béguin, A High-Performance Carbon for Supercapacitors Obtained by Carbonization of a Seaweed Biopolymer, *Adv. Mater.*, 2006, **18**, 1877–1882.
11 R. Cancelliere, *et al.*, Expanding the circularity of plastic and biochar materials by developing alternative low environmental footprint sensors, *Green Chem.*, 2023, **25**, 6774–6783.
12 E. Palmieri, R. Cancelliere, F. Maita, L. Micheli and L. Maiolo, An ethyl cellulose novel biodegradable flexible substrate material for sustainable screen-printing, *RSC Adv.*, 2024, **14**, 18103–18108.
13 S. Herou, P. Schlee, A. B. Jorge and M. Titirici, Biomass-derived electrodes for flexible supercapacitors, *Curr. Opin. Green Sustainable Chem.*, 2018, **9**, 18–24.

14 Z. Zhai, B. Ren, Y. Xu and Z. Liu, Metal-doped carbon aerogel from sodium alginate for supercapacitor, *IOP Conf. Ser.: Mater. Sci. Eng.*, 2019, **592**, 012077.
15 C. Cui, *et al.*, Recent Progress in Natural Biopolymers Conductive Hydrogels for Flexible Wearable Sensors and Energy Devices: Materials, Structures, and Performance, *ACS Appl. Bio Mater.*, 2021, **4**, 85–121.
16 E. Palmieri, *et al.*, A Sustainable Hydroxypropyl Cellulose-Nanodiamond Composite for Flexible Electronic Applications, *Gels*, 2022, **8**, 783.
17 F. Maita, *et al.*, Application of Unconditioned Nanostructured Thermoplastic-Based Strain Gauge Sensor in Wearable Electronics, *IEEE Sens. J.*, 2022, 1.
18 G. Landi, V. Granata, R. Germano, S. Pagano and C. Barone, Low-Power and Eco-Friendly Temperature Sensor Based on Gelatin Nanocomposite, *Nanomaterials*, 2022, **12**, 2227.
19 G. Landi, *et al.*, Regeneration and Long-Term Stability of a Low-Power Eco-Friendly Temperature Sensor Based on a Hydrogel Nanocomposite, *Nanomaterials*, 2024, **14**, 283.
20 G. Landi, *et al.*, Impact of Acetate-Based Hydrogel Electrolyte on Electrical Performance and Stability of Eco-Friendly Supercapacitors, *ChemElectroChem*, 2023, **10**, 1–10, DOI: 10.1002/celc.202300443.
21 G. Landi, L. La Notte, A. L. Palma and G. Puglisi, Electrochemical Performance of Biopolymer-Based Hydrogel Electrolyte for Supercapacitors with Eco-Friendly Binders, *Polymers*, 2022, **14**, 4445.
22 J. Menzel, E. Frąckowiak and K. Fic, Agar-based aqueous electrolytes for electrochemical capacitors with reduced self-discharge, *Electrochim. Acta*, 2020, **332**, 135435.
23 J. Zhao, *et al.*, Preparation of the polyelectrolyte complex hydrogel of biopolymers *via* a semi-dissolution acidification sol-gel transition method and its application in solid-state supercapacitors, *J. Power Sources*, 2018, **378**, 603–609.
24 W. Zhao, L. Wei, Q. Fu and X. Guo, High-performance, flexible, solid-state micro-supercapacitors based on printed asymmetric interdigital electrodes and bio-hydrogel for on-chip electronics, *J. Power Sources*, 2019, **422**, 73–83.
25 K. Wang, *et al.*, Electrodeposition of alginate with PEDOT/PSS coated MWCNTs to make an interpenetrating conducting hydrogel for neural interface, *Compos. Interfaces*, 2019, **26**, 27–40.
26 I. Babeli, *et al.*, Conductive, self-healable and reusable poly(3,4-ethylenedioxythiophene)-based hydrogels for highly sensitive pressure arrays, *J. Mater. Chem. C*, 2020, **8**, 8654–8667.
27 Y. Han and L. Dai, Conducting Polymers for Flexible Supercapacitors, *Macromol. Chem. Phys.*, 2019, **220**, 1800355.
28 G. Polino, *et al.*, Nanodiamond-Based Separators for Supercapacitors Realized on Paper Substrates, *Energy Technol.*, 2020, **8**, 1901233.
29 J. Collins, G. Gourdin and D. Qu, Modern Applications of Green Chemistry, *Green Chem.*, 2018, 771–860, DOI: 10.1016/B978-0-12-809270-5.00028-5.
30 L. Xia, L. Yu, D. Hu and G. Z. Chen, Electrolytes for electrochemical energy storage, *Mater. Chem. Front.*, 2017, **1**, 584–618.
31 L. Yu and G. Z. Chen, Ionic Liquid-Based Electrolytes for Supercapacitor and Supercapattery, *Front. Chem.*, 2019, **7**, 1–15, DOI: 10.3389/fchem.2019.00272.
32 J. Zeng, L. Wei and X. Guo, Bio-inspired high-performance solid-state supercapacitors with the electrolyte, separator, binder and electrodes entirely from: Kelp, *J. Mater. Chem. A*, 2017, **5**, 25282–25292.
33 R. Zhang, L. Wang, J. Zhao and S. Guo, Effects of Sodium Alginate on the Composition, Morphology, and Electrochemical Properties of Electrospun Carbon Nanofibers as Electrodes for Supercapacitors, *ACS Sustainable Chem. Eng.*, 2019, **7**, 632–640.
34 S. Brunauer, P. H. Emmett and E. Teller, Adsorption of Gases in Multimolecular Layers, *J. Am. Chem. Soc.*, 1938, **60**, 309–319.
35 G. Gupta, A. Diwedi, A. Sharma and K. Shandilya, Hierarchical NiMn Double Layered/Graphene with Excellent Energy Density for Highly Capacitive Supercapacitors, *Res. Rev.*, 2021, DOI: 10.21203/rs.3.rs-1188443/v1.
36 E. Taer, *et al.*, The relationship of surface area to cell capacitance for monolith carbon electrode from biomass materials for supercapacitor aplication, *J. Phys.: Conf. Ser.*, 2018, **1116**, 032040.
37 S. Zhu, *et al.*, Insights into the rheological behaviors evolution of alginate dialdehyde crosslinked collagen solutions evaluated by numerical models, *Mater. Sci. Eng., C*, 2017, **78**, 727–737.
38 I. Plazonić, I. Bates and Z. Barbaric-Mikocevic, The Effect of Straw Fibers in Printing Papers on Dot Reproduction Attributes, as Realized by UV Inkjet Technology, *BioResources*, 2016, **11**, 5033–5049.
39 K. Paszkowska, H. Podsiadlo and A. Ambroziewicz, Influence of the fibre composition of paper containing synthetic fibres on printing properties, *Pap. Technol.*, 2005, **46**, 21–29.
40 A. G. Pandolfo and A. F. Hollenkamp, Carbon properties and their role in supercapacitors, *J. Power Sources*, 2006, **157**, 11–27.
41 J. A. Baker, *et al.*, Development of Graphene Nano-Platelet Ink for High Voltage Flexible Dye Sensitized Solar Cells with Cobalt Complex Electrolytes, *Adv. Eng. Mater.*, 2017, **19**, 1600652.
42 R. Matshitse and T. Nyokong, Substituent effect on the photophysical and nonlinear optical characteristics of Si phthalocyanine – Detonated nanodiamond conjugated systems in solution, *Inorg. Chim. Acta*, 2020, **504**, 119447.
43 Q. Bai, Q. Xiong, C. Li, Y. Shen and H. Uyama, Hierarchical porous carbons from a sodium alginate/bacterial cellulose composite for high-performance supercapacitor electrodes, *Appl. Surf. Sci.*, 2018, **455**, 795–807.
44 H. J. Lomeri, *et al.*, Integration of a Paper-Based Supercapacitor and Flexible Perovskite Mini-Module: Toward Self-Powered Portable and Wearable Electronics, *Adv. Funct. Mater.*, 2024, **34**, 2313267.
45 S. Ahmadpour, J. Tashkhourian and B. Hemmateenejad, The effect of carbonaceous materials on faradaic and charging current contribution in carbon paste electrodes

investigated by chemometrics methods, *J. Solid State Electrochem.*, 2019, **23**, 3255–3266.

46 W. Pholauyphon, P. Charoen-amornkitt, T. Suzuki and S. Tsushima, Perspectives on accurately analyzing cyclic voltammograms for surface- and diffusion-controlled contributions, *Electrochem. Commun.*, 2024, **159**, 107654.

47 A. Patra, M. Shaikh, S. Ghosh, D. J. Late and C. S. Rout, MoWS2 nanosheets incorporated nanocarbons for high-energy-density pseudocapacitive negatrode material and hydrogen evolution reaction, *Sustainable Energy Fuels*, 2022, **6**, 2941–2954.

48 A. Patra, *et al.*, All-solid-state flexible supercapacitor based on a binary transition metal dichalcogenide grown on 2D/2D heterostructure materials, *J. Energy Storage*, 2023, **68**, 107825.

49 J. Zhang, M. Gu and X. Chen, Supercapacitors for renewable energy applications: A review, *Micro Nano Eng.*, 2023, **21**, 100229.

50 J. Deng, J. Li, S. Song, Y. Zhou and L. Li, Electrolyte-dependent supercapacitor performance on nitrogen-doped porous bio-carbon from gelatin, *Nanomaterials*, 2020, **10**, 353, DOI: 10.3390/nano10020353.

51 J. Landers, G. Y. Gor and A. V. Neimark, Density functional theory methods for characterization of porous materials, *Colloids Surf., A*, 2013, **437**, 3–32.